analytical chemistry

Article

pubs.acs.org/ac

Dissecting the Binding Mode of Low Affinity Phage Display Peptide Ligands to Protein Targets by Hydrogen/Deuterium Exchange Coupled to Mass Spectrometry

Ulrike Leurs,[#,†] Brian Lohse,[†] Shonoi Ming,[‡] Philip A. Cole,[‡] Rasmus P. Clausen,[†] Jesper L. Kristensen,[†] and Kasper D. Rand*[,#]

[#]Department of Pharmacy, University of Copenhagen, Universitetsparken 2, DK-2100 Copenhagen, Denmark

[†]Department of Drug Design and Pharmacology, University of Copenhagen, Universitetsparken 2, DK-2100 Copenhagen, Denmark

[‡]Department of Pharmacology and Molecular Sciences, Johns Hopkins University School of Medicine, 725 N. Wolfe Street, 316 Hunterian Bldg., Baltimore, Maryland MD21205, United States

Supporting Information

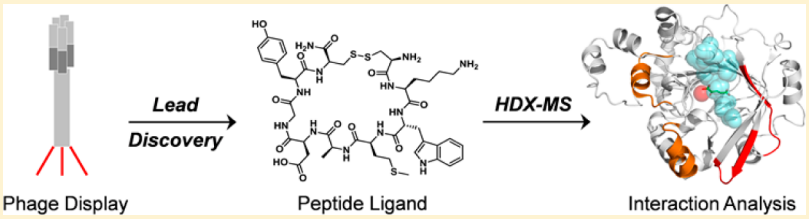

ABSTRACT: Phage display (PD) is frequently used to discover peptides capable of binding to biological protein targets. The structural characterization of peptide−protein complexes is often challenging due to their low binding affinities and high structural flexibility. Here, we investigate the use of hydrogen/deuterium exchange mass spectrometry (HDX-MS) to characterize interactions of low affinity peptides with their cognate protein targets. The HDX-MS workflow was optimized to accurately detect low-affinity peptide−protein interactions by use of ion mobility, electron transfer dissociation, nonbinding control peptides, and statistical analysis of replicate data. We show that HDX-MS can identify regions in the two epigenetic regulator proteins KDM4C and KDM1A that are perturbed through weak interactions with PD-identified peptides. Two peptides cause reduced HDX on opposite sides of the active site of KDM4C, indicating distinct binding modes. In contrast, the perturbation site of another PD-selected peptide inhibiting the function of KDM1A maps to a GST-tag. Our results demonstrate that HDX-MS can validate and map weak peptide−protein interactions and pave the way for understanding and optimizing the binding of peptide scaffolds identified through PD and similar ligand discovery approaches.

An estimated 40% of current pharmaceutical research focuses on the development of protein and peptide-based drugs.[1] Phage display (PD) allows the easy and rapid discovery of protein and peptide binders to biological targets that may be developed into drugs. Through sequential enrichment of large DNA-encoded phage libraries, the proverbial "needle-in-the-haystack" interacting with a given target can be identified.[2] Peptides identified by PD often bind to biologically important sites of the protein, such as the active site of an enzyme, and are hence good drug candidates. Beyond competitive inhibition via active site interactions, the sequence and/or tertiary structure of the selected peptides can also behave as allosteric modulators of the target protein. These allosteric modulator peptides sometimes mimic natural allosteric binding proteins, exemplifying a phenomenon known as "convergent evolution".[3]

Unfortunately, many hits from PD screening do not show satisfactory affinity *in vitro*, though it has been estimated that PD selected peptides must bind to their protein target with a dissociation constant of 50 μM or lower in order to endure the vigorous washing steps during biopanning.[4] The reduced affinity of the synthetic peptide versus the corresponding phage can be due to the loss of multivalency. The commonly employed M13 phage displays peptides via its pIII coat protein in 3−5 copies,[5] and the possibility that the peptide−protein interaction is driven not only by the monomeric peptide sequence but also by its multimeric presentation on the phage has been discussed extensively.[6] Indeed, a recent study showed that the tetrameric presentation of a PD selected peptide exhibited 45-fold higher binding affinity toward the target when compared to the monomeric peptide.[7]

As peptides encoded by phage libraries are normally 10−20 amino acids long, they usually do not adopt a stable secondary structure in solution but are conformationally mobile.[8] Due to their high structural flexibility, it is often challenging to identify peptide binding epitopes on proteins by conventional X-ray

Received: August 21, 2014
Accepted: October 17, 2014
Published: October 17, 2014

   dx.doi.org/10.1021/ac503137u | *Anal. Chem.* 2014, 86, 11734−11741

crystallography. In addition, the weak binding constants of phage display derived peptide ligands to their target proteins require a large excess of the weak binding peptide ligands which might interfere with crystal formation.[9] While the advantages and information content of X-ray crystallography are undisputed, new analytical tools are needed to dissect the binding mode of weak binding and structurally flexible peptides and to identify false-positive hits from high-throughput screenings originating, e.g., from binding artifacts and nonspecific interactions. Furthermore, perturbations in protein dynamics upon peptide binding are not readily detected due to the rigidity of crystal structures.

The hydrogen/deuterium exchange (HDX) of proteins provides a sensitive window into the molecular interactions and dynamics of proteins in solution. Coupling of HDX with mass spectrometric detection (MS) has within recent years evolved to be a popular choice to study protein−protein interactions and transient protein folding states.[10,11] Through HDX-MS, the exchange of backbone amide hydrogens for deuteriums can be localized to different regions of a protein by pepsin proteolysis of the deuterium labeled protein. Perturbations to the conformation of a protein upon peptide binding, through either direct interaction or indirect changes in dynamics, can be detected by HDX-MS. A "perturbation site" typically manifests itself by localized reductions in deuterium uptake between the ligand-bound and the ligand-unbound protein.

Here, we describe and exemplify the tailoring of HDX-MS methodology to detect and map the perturbation sites of low affinity peptide ligands on target proteins in solution. HDX-MS is used to validate hits from phage display screening and detect and map the low affinity interaction of three inhibitory peptides (Peptides 1−3, Table 1) with two target proteins, KDM4C and KDM1A, which are involved in epigenetic regulation. The results demonstrate that HDX-MS can probe and validate weak (micromolar K_D) interactions of the PD-derived peptide ligands with their target proteins. Rigorous analysis of replicate HDX-MS data and comparison to a nonbinding peptide allow for the accurate detection of low-affinity binding events and ligand-induced structural rearrangements in the target protein.

Table 1. Peptide Sequences Including Modifications

peptide	sequence	protein
1[a]	Ac-NH-SHSEFWDWGPGGG-$CONH_2$	KDM1A
2[b]	NH_2-ACYTRNMNQC-$CONH_2$	KDM4C
3[c]	NH_2-CKWMADGYC-$CONH_2$	KDM4C
4[d]	NH_2-ACKWMDDGYCGGG-$CONH_2$	KDM4C

[a]Linear peptide. [b]Cyclized between Cys2 and Cys10 by *m*-xylene. [c]Cyclized between Cys1 and Cys9 by a disulfide bridge. [d]Cyclized between Cys2 and Cys10 by a disulfide bridge.

EXPERIMENTAL SECTION

Hydrogen/Deuterium Exchange Mass Spectrometry. The peptides were preincubated with KDM4C (expressed and purified as described elsewhere[12]) or GST-KDM1A (expressed and purified as described elsewhere[13]) for 30 min in order to allow target binding prior to deuterium labeling. Continuous amide $^1H/^2H$ hydrogen exchange (HX) was initiated by a 10-fold dilution of a protiated protein stock solution in the presence or absence of ligand into the corresponding deuterated buffer (HEPES (12.5 mM, pH 7.4), $FeSO_4$ (5 μM), ascorbate (100 μM)). Nondeuterated controls were prepared by dilution into an identical protiated buffer. All HDX reactions were carried out at room temperature and contained KDM4C (1.2 μM) or KDM1A (0.8 μM) in the absence or presence of peptide (160 μM). At appropriate time points (ranging from 15 s to 8 h), aliquots of the HDX reaction were quenched by addition of an equal volume of ice-cold quenching buffer (containing TRIS (1.25 M, pH 2.15) and TCEP (125 mM) for KDM4C and TRIS (1.25 M, pH 2.15), guanidine (6 M), and TCEP (250 mM) for GST-KDM1A) resulting in a final pH of 2.3. Quenched samples were immediately frozen and stored at −80 °C. Samples were injected into a cooled Waters nanoAcquity UPLC system for online pepsin digestion and rapid desalting of the protein samples. After digestion of the samples, the peptic peptides were trapped on a precolumn (Waters VanGuard C18, 1.7 μm, 2.1 × 5 mm, Milford, MA, USA) and desalted with 0.68% formic acid, pH 2.3, 150 μL/min for 3 min. Peptides were eluted from the trap to the analytical column (Waters XBridge C18, 1.7 μm, 1.0 mm × 100 mm) and separated with an 8−40% gradient of 0.68% formic acid in acetonitrile (pH 2.3) over 12 min at a flow rate of 40 μL/min. Positive ion-electrospray ionization mass spectra of eluted peptides were acquired on a Waters SynaptG2 HDMS mass spectrometer. Peptic peptides were identified in separate experiments using collision-induced dissociation tandem mass spectrometry performed with a data-independent (MS^E) acquisition scheme. Sequence coverage maps of peptic peptides of KDM4C and GST-KDM1A are shown in Figures S4 and S5, Supporting Information. The sequence coverage was 91.7% with a redundancy of 1.84 for KDM4C and 92.6% with a redundancy of 1.61 for KDM1A. Mass spectra were processed using the MassLynx and DynamX software packages (Waters Corp.); bimodal curve fitting was performed using HX-Express.[14] Complete deuteration of control samples was achieved by incubation of 60 pmol of KDM4C (40 pmol KDM1A) in the deuterated buffer in the presence of 6 M guanidine for 24 h at 30 °C. Average back exchange (i.e., deuterium loss) was measured as 37%. However, no corrections were made for this deuterium loss as only the relative levels of deuterium incorporation of all samples were compared. The HDX of KDM4C in the presence and absence of peptide after a 10 min exchange was measured in triplicate to confirm the significance of the detected changes in deuterium uptake. Changes in deuterium uptake were considered significant if they exceeded the triple standard deviation and/or passed a two-tailed, unpaired *t*-test ($p < 0.05$). Protein structures were visualized using PyMOL (DeLano Scientific). ETD-HDX-MS was performed as described elsewhere.[15] For each ETD experiment, 240 pmol of KDM4C was preincubated with 3.42 nmol of peptide 2 for 30 min and then diluted 10-fold into deuterated buffer. The absence of H/D scrambling was monitored by examining the deuterium uptake of the charge-reduced and the deammoniated ion species.[16] ETD was performed in the trap traveling wave ion guide using 1,4-dicyanobenzene as the ETD reagent (Sigma-Aldrich, St. Louis, USA).

Peptide Synthesis and Testing. Peptide 1 was purchased from GenScript USA Inc. (NJ, USA); the purity was stated by the manufacturer to be >95%. Peptides 2 and 3 were synthesized, purified, and characterized as described elsewhere.[17] The peptide sequences are shown in Table 1. For inhibition studies on KDM1A, a peroxidase-coupled assay monitoring hydrogen peroxide production was performed as

dx.doi.org/10.1021/ac503137u | *Anal. Chem.* 2014, 86, 11734−11741

Scheme 1. General Workflow for the Integration of PD Lead Discovery and Interaction Analysis of Peptides and Proteins by HDX-MS[a]

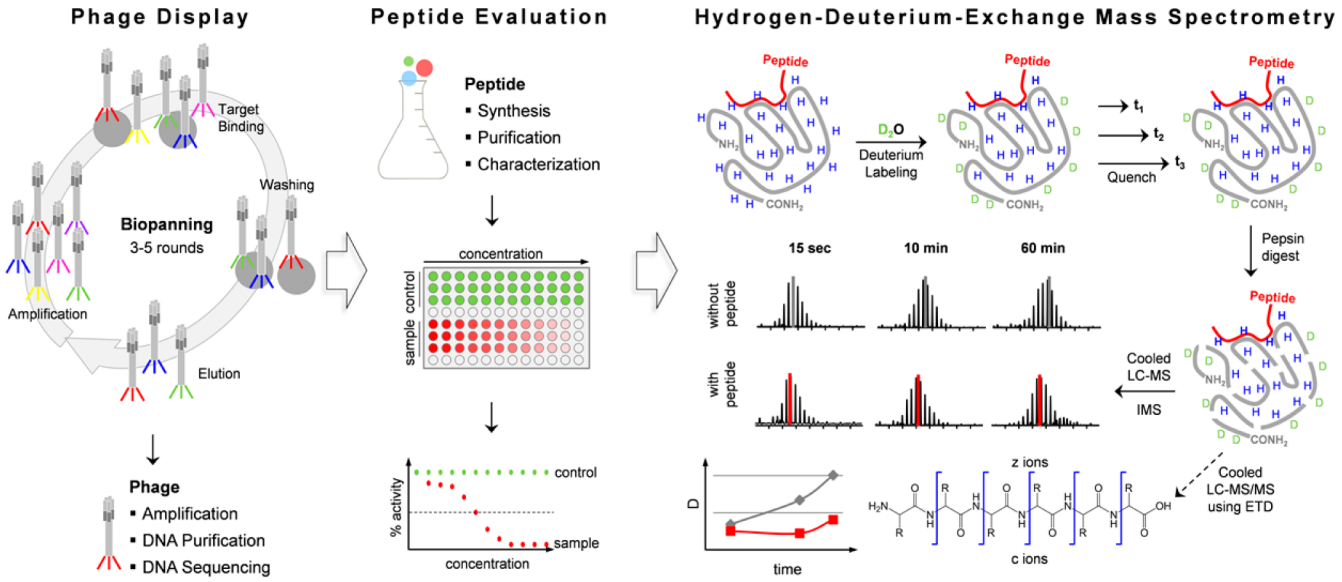

[a]Over 3−5 rounds of biopanning, PD can enrich for one, or several, peptide−phages interacting with the immobilized target protein. The binding peptide sequences are obtained by DNA sequencing of the enriched phages, subsequently chemically synthesized, and then tested for their *in vitro* activity towards the target protein. Interaction analysis is then performed between the peptide leads and the target protein by HDX-MS. Briefly, HDX is initiated by diluting the protein in the presence or absence of peptide into a deuterated buffer, and after different periods of deuterium labeling, samples are taken and quenched. The deuterated samples are then digested, and the peptic peptides are analyzed by LC-MS and LC-MS/MS. Differential deuterium uptake plots indicate a binding event (grey curve, free protein; red curve, peptide-bound protein). The resolution of HDX-MS can be narrowed down from peptic peptide to single amino acid level by ETD gas-phase fragmentation.[36]

previously described.[18] KDM1A expression and purification was carried out as described elsewhere;[13] non-GST-tagged KDM1A was purchased from BPS Biosciences (#50097). The time courses of the reaction were measured under aerobic conditions using a Beckman Instruments DU series 600 spectrophotometer equipped with a thermostat-controlled cell holder (T = 25 °C). The 100 μL reactions were initiated by addition of enzyme (100−200 nM) to the reaction mixture (HEPES buffer (50 mM, pH 7.5), 4-aminoantipyrine (0.1 mM), 3,5-dichloro-2-hydroxybenzenesulfonic acid (1 mM), horseradish peroxidase (0.76 μM, Worthington Biochemical Corp.), peptide 1 (100 μM), and H3K4me2 histone peptide substrate (24 μM)). Absorbance changes were monitored at 515 nm, and an extinction coefficient of 26 000 $M^{-1}\cdot cm^{-1}$ was used to calculate product formation. For curve fitting and data analysis, GraphPad Prism 6.0 was used.

RESULTS AND DISCUSSION

Workflow Optimization for the Detection of Low Affinity Peptide/Protein Interactions by HDX-MS. The general workflow for the discovery, validation, and analysis of peptides by PD and HDX-MS is depicted in Scheme 1. The traditional HDX-MS workflow for protein−ligand analysis had to be adapted to allow the analysis of low affinity peptide/protein interactions. Previously published protocols for HDX-MS of protein−ligand interactions utilize 5−10 times excess of ligand over protein.[19,20] However, these conditions are optimized for nano- or picomolar affinities between ligand and protein; the affinities of the peptide ligands tested here were in the micromolar range. Theoretical calculations estimating the percentage of protein-bound peptide from its IC_{50} value revealed that a 130-fold molar excess of peptide compared to the protein had to be used to ensure sufficient occupancy of the protein with peptide. Further, the samples were allowed to preincubate for 30 min at room temperature prior to deuterium labeling to ensure equilibrium binding of the peptide to the protein. Unfortunately, the large amount of peptide (5−15 μg per run) led to overloading of the chromatographic system and resulted in increased carryover between the chromatographic runs. An extensive washing procedure consisting of three serial gradients flushing the column of excess peptide had to be implemented to decrease the carryover. In addition, we found that the vast excess of peptide resulted in ion suppression; the quantitative analysis of 19 different peptic peptides covering the whole protein sequence of KDM4C revealed that 80% of the signal intensities were lost upon peptide addition. Hence, higher protein concentrations had to be used to ensure sufficient sequence coverage upon ligand addition. Further, PD-derived peptides are prone to proteolytic cleavage by pepsin because they often have an unusually high content of aromatic amino acids.[21] This is due to the fact that the active site of an enzyme is often composed of a hydrophobic cleft, and the free energy gained by burying aromatic residues in this cleft drives the binding of the peptides.[22] For instance, peptic cleavage of one of the peptide ligands resulted in truncated peptides that interfered with detection of peptides from the target protein. In addition, signal overlap from the multiplicity of peptic peptides from the protein sample and synthesis impurities from the ligand sample can give rise to interference. To circumvent these challenges, we made use of orthogonal gas-phase separation of the peptide ligand from the target protein peptides by ion mobility. Ion mobility spectrometry (IMS) separates analyte ions in a drift tube filled with a carrier gas in the presence of an electrical field.[23] The analytes' mobility in the drift tube depends on its mass, size, charge, and shape. The utility of coupling IMS to the

dx.doi.org/10.1021/ac503137u | *Anal. Chem.* 2014, 86, 11734−11741

HDX-MS workflow has been demonstrated previously;[24] here we found the increased separation capability particularly useful in HDX-MS analyses of weak peptide−protein interactions. As an example, Figure 1 shows a singly charged peptide ion of

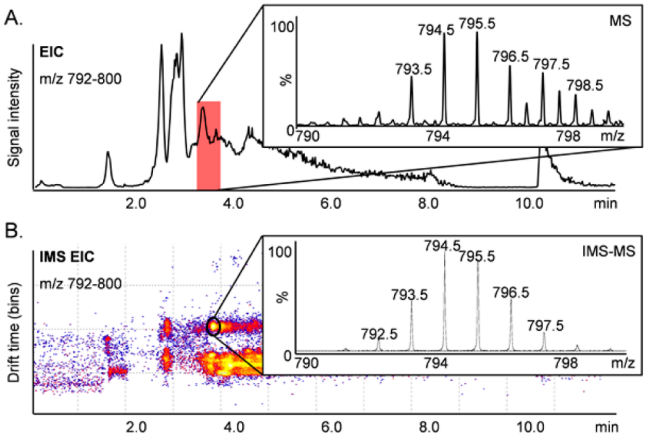

Figure 1. EIC (A) and corresponding ion mobility spectrum (B) of the KDM4C peptic peptide 113−120. The 1+ cluster of the peptide overlaps with a 2+ cluster originating from the protein/peptide sample. The insets show the mass spectra integrated over the indicated chromatographic range.

interest from KDM4C with an overlapping doubly charged peptide ion (not identified). The extracted ion chromatogram (EIC) shows the overlapping species coeluting after 3.8 min (Figure 1A). As shown in the right panel of Figure 1, the 2+ cluster overlaps with the 1+ cluster, making the accurate measurement of average mass impossible. Conventional chromatography failed to isolate the two species; however, the use of IMS led to full separation of these species due to different drift times (Figure 1B).

When analyzing weak peptide−protein interactions with dissociation constants in the micromolar range by HDX-MS, even a large excess of peptide will not result in a fully bound population of protein to ligand at equilibrium. Depending on the concentrations and the dilution factor upon initiation of the HDX reaction, the labeling reaction will typically only be possible with 50−75% of the protein in the ligand-bound state. Thus, changes in HDX resulting from ligand binding will be scaled down, and the reductions in deuterium uptake upon binding of low affinity peptide ligands are likely to be small in magnitude. To account for this, our optimized HDX-MS workflow dictates a comprehensive statistical analysis from replicate experiments, allowing the identification of all sites that display protection effects from HDX, even if they are minor (<0.5 D). In the cases of KDM4C and KDM1A described here, changes in HDX ranged from 0.2 to 2 D upon ligand interaction. In our protocol, we consider changes in deuterium uptake to be significant if they exceeded the triple standard deviation and/or passed a two-tailed, unpaired *t*-test ($p < 0.05$). We find that these threshold values are in good agreement with a previously published study that investigates a nonpeptidic ligand binding to microtubulin.[25]

HDX-MS Analysis of the Interactions of Peptide Ligands with the Histone Demethylases KDM1A and KDM4C. We recently reported the discovery of several peptide ligands binding to the two histone demethylases KDM1A and KDM4C by phage display.[17] The crystal structures of KDM1A and KDM4C are shown in Figure 2. KDM1A belongs to the

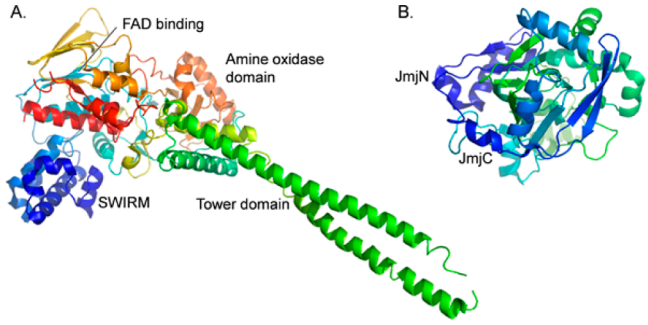

Figure 2. Structural models of the peptide ligand targets KDM1A (A, pdb 2Z3Y) and KDM4C (B, pdb 2XML) as determined by X-ray crystallography.

family of flavin-dependent monoamine oxidases and contains a SWIRM domain, a FAD-binding motif, and an amino oxidase domain, as well as a tower domain which promotes binding to the transcription factor CoREST.[26] KDM4C is a jumonji-domain containing protein consisting of an N-terminal JmjN and a JmjC domain, as well as two C-terminal PHD and Tudor domains.[27] In this study, a truncated, $(His)_6$-tagged version of KDM4C was used, only containing the catalytic core domains JmjN and JmjC. The KDM1A protein was expressed with an N-terminal GST-tag.

Through 4−5 rounds of biopanning against $(His)_6$-ccKDM4C and GST-KDM1A, phage display led to the discovery of one peptide binding to KDM1A and two further peptides interacting with KDM4C. These peptides were optimized to improve their inhibitory activity on the target proteins and their druggability; two of the second generation peptides targeting KDM4C, as well as a first generation peptide directed against KDM1A, were used in this study for HDX-MS analysis, workflow development, and optimization (Table 1).

Histone Demethylase KDM4C. We recently identified two peptides (2 and 3, Table 1) interacting with KDM4C by PD.[17] In an *in vitro* TR-FRET demethylase assay, the inhibition constants of these peptides were found to be in the high μM range. In a cell-based assay, none of the peptides showed any inhibitory activity, most probably due to insufficient cellular uptake. In order to design more cell-permeable peptidomimetics, we set out to determine the crystal structure of the peptides in complex with KDM4C. Despite extensive efforts, no crystals containing the peptides could be obtained; therefore, their binding sites were investigated by HDX-MS. Four different sites on KDM4C showed altered deuterium uptake upon peptide addition, and an alanine scan revealed functionally important amino acids in the peptide ligands. On the basis of these findings, the initial peptide leads were truncated and structure optimized, and these second generation peptide ligands (peptides 2 and 3) displayed an apparent increase in activity by 10-fold.[17] Here, we describe how HDX-MS can be used for a comprehensive, in-depth investigation of the differences between the initial hits from the PD and the second generation peptide ligands. Changes in peptide binding mode and target engagement are analyzed and validated using our tailored HDX-MS protocol.

The mode of interaction between peptides 2 and 3 and KDM4C was studied by HDX-MS and revealed that both peptides led to a reduction of deuterium uptake along the KDM4C sites 113−120 (A) and 166−174 (B); while peptide 3 additionally reduced deuterium uptake of the neighboring α-

dx.doi.org/10.1021/ac503137u | *Anal. Chem.* 2014, 86, 11734−11741

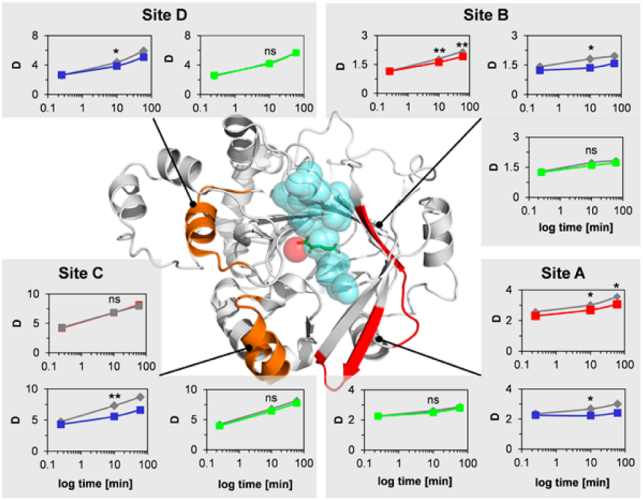

Figure 3. Deuterium uptake plots of sites 113−120 (A), 166−174 (B), 248−275 (C), and 331−344 (D) of peptides 2 (red), 3 (blue), and 4 (green) against free KDM4C (gray curves). The crystal structure shows KDM4A (pdb 2VD7) in complex with histone peptide substrate (blue spheres) and the catalytic Fe^{2+} ion (red sphere); sites A and B are colored red; sites C and D are shown in orange ($n = 3$; ∗, $p < 0.05$; ∗∗, $p < 0.01$).

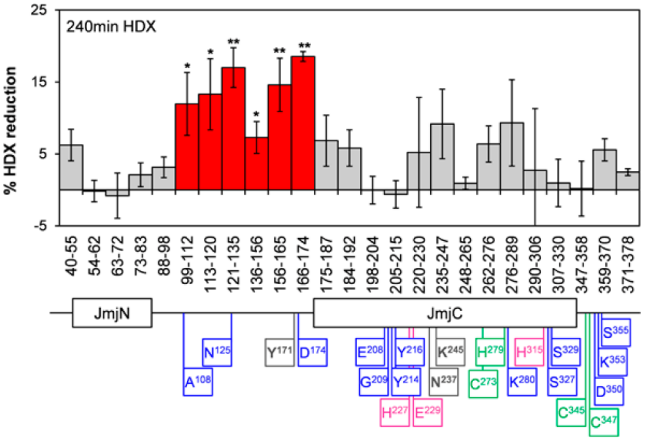

Figure 4. Differential HDX-MS data for KDM4C ± peptide 2. The domain structure of the catalytic core of KDM4C is indicated below the *x*-axis; the amino acids critical for 2-OG binding are highlighted in gray, residues involved in Fe^{2+} coordination are pink, Zn^{2+} coordinating residues are green, and residues involved in substrate binding and/or catalytic activity are indicated in blue ($n = 3$, error bars are standard deviation of the mean; ∗, $p < 0.05$; ∗∗, $p < 0.01$).

helical regions 248−275 (C) and 331−344 (D) (Figure 3). No reduction of deuterium uptake was observed along site C in the presence of peptide 2. The significance of these results was verified through triplicate measurements after 10 min of deuterium labeling in the presence and absence of peptide ligand. Table S1, Supporting Information, shows the numerical values of differential deuterium uptake and their standard deviations after 10 min HDX.

To exclude the possibility that the detected changes are due to nonspecific binding events related to the high peptide concentrations employed during the labeling reaction, we have used the additional, noninhibitory peptide 4 (Table 1) to control for nonspecific binding. No significant differences in deuterium uptake levels along the sites of interest were observed upon addition of peptide 4 (Figure 3 and Table S1, Supporting Information), confirming that the observed effects indeed result from specific interactions between peptides 2−3 and KDM4C.

To further probe and reveal the full impact of peptide 2 on KDM4C conformation and dynamics, we performed a triplicate HDX-MS analysis of the KDM4C-peptide 2 complex across a longer HDX time range (up to 480 min). Furthermore, a comprehensive statistical analysis of all data was applied to detect small yet significant perturbations in HDX upon ligand binding. Figure 4 shows an overview of all analyzed peptides after 240 min of HDX where significance was defined as changes in deuterium uptake that are bigger than the triple standard deviation and a $p < 0.05$ in an unpaired, two-tailed *t*-test. The complete deuterium uptake curves ± peptide 2 are shown in the Supporting Information (Figure S1). Using this procedure, several additional sites, 99−112, 121−135, 136−156, 156−165, and 359−370, were identified in the vicinity of primary identified sites with significantly perturbed HDX in the presence of peptide 2. Some of those reductions in HDX were only significant after 240 min of HDX, and the additional time point (480 min) was used to further verify their validity (data not shown). When mapped onto the crystal structure of KDM4C, it becomes obvious that these peptides lay in between the initially identified sites A and B and C and D that show perturbed HDX upon ligand interaction (Figure S2, Supporting Information). For the two peptic peptides KDM4C99-105 and KDM4C104-112, overlapping with site 99−112, observed changes in HDX were not significant due to an elevated standard deviation (Figure S1, Supporting Information) and the protection effects could not be confirmed after 480 min due to poor data quality. These observations emphasize the importance of using significance analysis when assessing HDX-MS data from low affinity ligand binding experiments. Furthermore, the perturbation in HDX along site 359−370 was only significant after 10 min (Figure S1, Supporting Information).

The peptic peptides reaching from 99−174 lay within a functionally unassigned region between the JmjN and the enzymatically active JmjC domain of KDM4C (Figure 4). The other two peptic peptides showing perturbations in HDX upon ligand interaction, KDM4C331−344 and 359−370, are partially located within the JmjC domain.[28,29] Except for Ala_{108}, Asn_{125}, and Asp_{174}, none of the functionally important residues of KDM4C overlap with these peptides. This indicates that the peptides are not inhibiting KDM4C through substrate competition, a hypothesis that is supported by the atypical inhibition kinetics displayed by analogues of peptides 2 and 3.[17] Instead, it can be hypothesized that the peptides bind to regions involved in protein−protein interaction on the surface of KDM4C by structurally mimicking interacting proteins. Actually, many epigenetic enzymes are known to interact with numerous other proteins; e.g., KDM4C is known to bind the histone deacetylases HDAC1 and −3,[30] and various other proteins have been implicated for KDM4C interaction, supporting this assumption. The discovery of peptides mimicking protein−protein interactions by phage display is a well-known phenomenon termed convergent evolution.[3]

Peptide 2 was derived and optimized from an initial phage display peptide scaffold reported previously.[17] The optimization of peptide 2 included the truncation of the peptide scaffold and the insertion of *m*-xylene into the disulfide bridge. While the initial PD peptide significantly reduced deuterium uptake along site D similar to peptide 3 (data not shown), a close inspection

dx.doi.org/10.1021/ac503137u | *Anal. Chem.* 2014, 86, 11734−11741

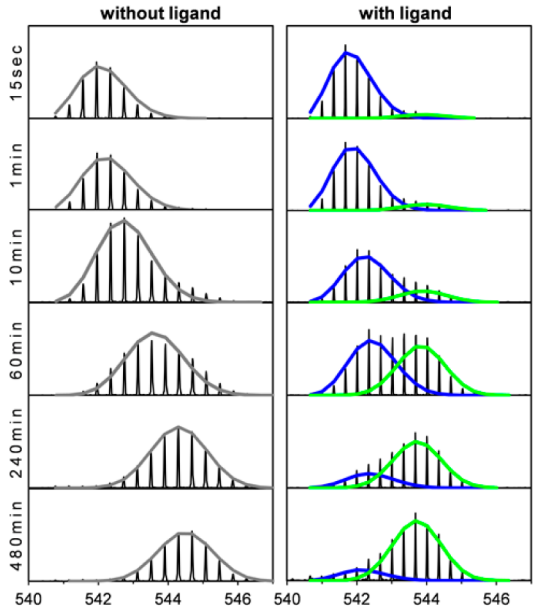

Figure 5. Mass spectra of KDM4C peptic peptide 331−344 in the absence and presence of peptide 2 after different times of HDX. The spectra without ligand were fitted to a binomial and the spectra with ligand to a bimodal peak distribution.

of HDX raw data revealed that peptide 2 induced unusual HDX kinetics in site D of KDM4C. Site D (331−344) displayed a pronounced bimodal isotopic distribution in the presence of peptide 2 (Figure 5) indicating the occurrence of two distinct conformations in this region of KDM4C that interconvert with slow dynamics (EX1 kinetics).[31] Neither the original phage display hit nor peptide 3 led to such pronounced bimodal patterns in site D. To confirm that the observed EX1 phenomenon was not due to sample carryover from previous chromatographic runs,[32] an optimized protocol consisting of 4 consecutive washing steps and a subsequent blank was introduced to monitor and minimize sample carryover. After this optimization, the inter-run carryover for peptide 331−344 was reduced to >0.5%, verifying that the observed peak broadening is indeed due to EX1 exchange kinetics.

Duplicate analysis of a full HDX time course in the presence and absence of peptide 2 according to the optimized protocol confirmed the occurrence of EX1 kinetics in the presence of peptide 2 with a good fit to a bimodal model and a change in peak width of 4.1 ± 0.4 m/z. We note that a slight broadening of the peak in the absence of ligand is observed around 60 min, yet this data had a good fit to a standard binomial distribution and did not fit adequately to a bimodal distribution.[14] Thus, the occurrence of two distinct populations (Figure 5) upon peptide binding suggests that peptide 2 induces slow unfolding dynamics in this region. An alternate explanation for the bimodal peak pattern could be slow binding kinetics of peptide 2 (slow k_{on}), a phenomenon that has been observed previously.[33,34]

To sublocalize residues in site D involved in EX1 kinetics upon peptide 2 interaction, the peptic peptide KDM4C331−344 was analyzed by electron transfer dissociation (ETD) tandem mass spectrometry. It has recently been shown that gas-phase fragmentation by ETD can be incorporated into the HDX-MS workflow to allow extraction of HDX information for individual amino acid residues in proteins.[35,36] The peptic peptide KDM4C331−344 fragmented sufficiently to allow a comprehensive analysis of deuterium uptake at single amino acid level. The c-ion series c_4−c_{11} revealed that the perturbed sites involved in EX1 kinetics in the presence of peptide 2 are

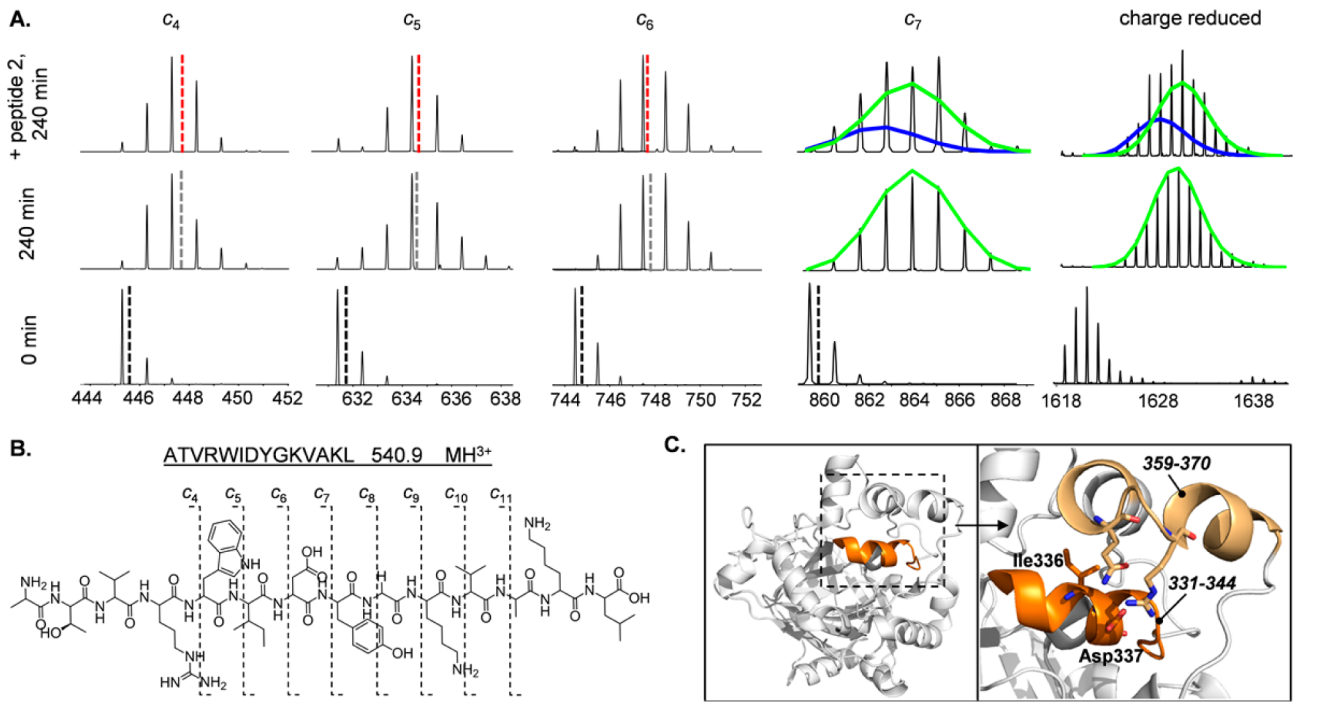

Figure 6. HDX-ETD analysis of site 331−344. (A) ETD fragment ion spectra after 0 and 240 min HDX ± peptide 2. The average mass is indicated by dashed lines. For the charge reduced species and the c_7 ion, the raw data were fitted to a bimodal distribution using HXExpress (population 1: blue curves; population 2: green curves). (B) Chemical structure and observed fragment ions of KDM4C331−344. (C) Crystal structure of KDM4C (pdb 2XML) with peptide 331−344 highlighted in orange and 359−370 in light-orange. Residues Ile336 and Asp337 are displayed as sticks.

dx.doi.org/10.1021/ac503137u | Anal. Chem. 2014, 86, 11734−11741

located in the vicinity of residue Asp337 (Figure 6A). The irregular isotopic distribution in the c_7 fragment ion spectrum indicates that EX1 kinetics occur from Asp337 toward the C-terminus of the peptide (Figure 6A,C). This region of 331−344 is buried underneath helix 359−370 and points toward that neighboring helix. Helix 359−370 shows reduced HDX (significant only after 10 min; see Figure S1, Supporting Information) but no EX1 exchange kinetics (data not shown). Likely, ligand interaction induces slow folding/refolding EX1 kinetics in the underlying helical region 331−344 in an indirect manner through helix 359−370. The ETD data support this hypothesis, as the C-terminal half of helix 331−344 observed to undergo slow unfolding dynamics upon peptide 2 interaction is in the closest vicinity of helix 359−370 (Figure 6C).

Three residues in helix 359−370 settle in a box-like arrangement (pygo-box), similar to the PHD finger of hPygol that recognizes tri- and dimethylated H3K4 residues. It has been hypothesized that the trimethylated K4 residue of H3 is in the proximity of this pygo-box; however, a conformational change in the C-terminal domain of the KDM4 family of proteins is required to accommodate the complete substrate. Our results appear to corroborate this hypothesis, as the observed EX1-type kinetics indicate that this part of the C-terminal domain of KDM4C possesses unusual conformational flexibility, which in turn could help facilitate the binding of other histone substrates than tri- and dimethylated H3K9.[37]

Histone Demethylase KDM1A. PD identified peptide 1 as a binder of GST-KDM1A, and the resynthesized peptide showed mixed inhibition of GST-KDM1A in an *in vitro* demethylase activity assay (Figure S3A, Supporting Information). Analysis of the binding of peptide 1 to GST-KDM1A using our optimized HDX-MS workflow revealed decreased deuterium uptake along region 101−114 (Figure 7B,D). Interestingly, this site resides in the GST-tag, implying that peptide 1 effectively does not interact with KDM1A but rather with the GST protein fused to the N-terminus of KDM1A for purification purposes. No other peptides covering the sequence of KDM1A displayed changes in deuterium uptake upon peptide addition (an example is shown in Figure 7A,C). To validate our findings from HDX-MS, a cross-affinity ELISA of the peptide-1-phage against recombinant GST protein was performed, showing that the peptide-1-phage indeed binds the GST protein (Figure S3C, Supporting Information). This confirms that the interaction between KDM1A101−114 and peptide 1 detected by HDX-MS is not an artifact. Furthermore, the inhibitory activity of peptide 1 was reassessed using recombinant KDM1A protein without a GST-tag, and no inhibitory activity of peptide 1 could be detected for this KDM1A construct (Figure S3B, Supporting Information). The inhibitory activity of peptide 1 toward GST-KDM1A can probably be explained on the basis of the close proximity of the GST-tag to the N-terminus of KDM1A; the binding site 101−114 is thereby located next to the actual KDM1A protein.

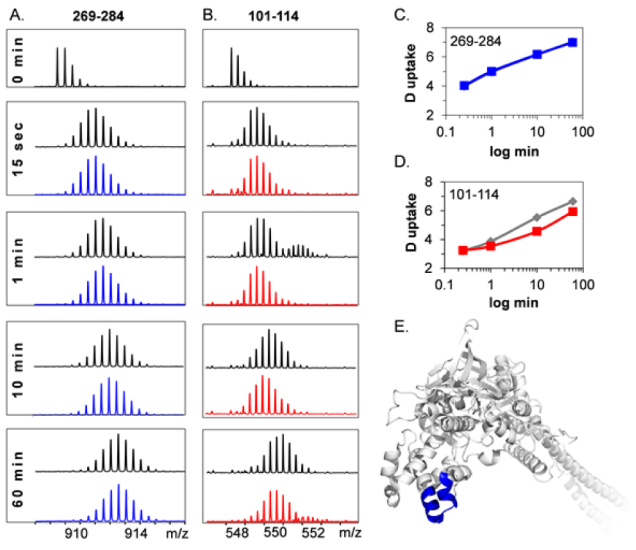

Figure 7. Mass spectra of KDM1A peptic peptides 269−284 (A) and 101−114 (B) in the absence (black) and presence (red/blue) of peptide 1 after different times of HDX. Deuterium uptake plots of 269−284 (C) and 101−114 (D); gray curves indicate the deuterium uptake in the absence of peptide 1, and red/blue curves indicate deuterium uptake in its presence. (E) The α helix highlighted in blue represents KDM1A269−284 (pdb 2Z3Y).

The example of GST-KDM1A illustrates the identification of a peptide ligand by phage display that inhibits the target protein *in vitro* without actually interacting with it. Though purification tags are an important tool in protein biochemistry and especially the fusion of proteins with GST can assist protein solubilization and stability,[38] our findings emphasize the benefit of using small or cleavable purification tags for proteins employed in drug discovery. Furthermore, identified interactors of proteins should always be validated using different methods and/or different constructs of the protein. Our findings are in accord with a previously published study showing that large purification tags can influence protein structure and activity and thereby lead to the identification of false-positives.[39]

CONCLUSIONS

Here, we report the optimization and validation of an HDX-MS workflow to dissect the binding modes of phage display-derived low-affinity peptide ligands on their target proteins. Using a panel of peptide ligands binding to the two epigenetic regulator proteins KDM4C and KDM1A, we exemplify the advantages and challenges of combining these two technologies. Our results show that HDX-MS can provide an alternative analytical tool for validating and optimizing drug scaffolds from high-throughput screening methods such as phage display. The workflow was optimized by implementation of IMS and ETD to achieve better sensitivity as well as the use of a nonbinding control peptide and statistical analysis of replicate data. As shown by the example of KDM4C, several hits from phage display and/or optimized peptide lead structures can be analyzed and compared to each other. By combining HDX-MS with ETD fragmentation, higher resolution information can be obtained to explicitly study changes in dynamics as a consequence of ligand interaction as we show here for peptide 2 binding to KDM4C. To our knowledge, the data presented here is the first example of the use of ETD to sublocalize residues involved in slow conformational dynamics (EX1-type kinetics) in a protein−ligand complex. There are some advantages of this HDX-MS workflow compared to, i.e., X-ray crystallography: For instance, a few hundred pmol of protein and 1 mg of peptide will often be sufficient to conduct and obtain HDX data on a protein-peptide interaction. The effects of peptide binding to the protein are measured in the solution phase and therefore more closely reflect native conditions for the target protein. Both direct and indirect dynamic effects on the target protein conformation upon ligand binding are detected. In effect, HDX-MS reveals the "dynamic"

binding site on the target protein, which provides a solution-phase view of all backbone amide sites perturbed by peptide interaction. The example of KDM1A shows how HDX-MS can be used to validate hits from phage display and identify false-positives. Finally, it should be noted that the method is quite tolerant to molecular size, also allowing the analysis of large complexes such as antibodies binding to protein targets.

In summary, HDX-MS can be used to study low affinity peptide/protein interactions that are not accessible by traditional structure elucidation techniques. Our findings indicate that HDX-MS can provide a much-needed alternative analytical tool to understand the conformational dynamics of weak peptide−protein interactions important in both chemical biology research and early stage drug development.

■ ASSOCIATED CONTENT

Supporting Information

Additional information as noted in the text. This material is available free of charge via the Internet at http://pubs.acs.org.

■ AUTHOR INFORMATION

Corresponding Author

*E-mail: Kasper.Rand@sund.ku.dk.

Notes

The authors declare no competing financial interest.

■ ACKNOWLEDGMENTS

We gratefully acknowledge financial support from the Marie Curie Actions Programme of the EU (Grant No. PCIG09-GA-2011-294214) and the Danish Council for Independent Research Natural Sciences (Steno Grant No. 11-104058). This work was furthermore supported by Danish Cancer Society and the NIH.

■ REFERENCES

(1) Rader, A. R. *BioProcess Int.* **2013**, *11*, 7.
(2) Smith, G. P. *Science* **1985**, *228*, 1315−1317.
(3) Kay, B. K.; Kasanov, J.; Knight, S.; Kurakin, A. *FEBS Lett.* **2000**, *480*, 55−62.
(4) Kay, B. K.; Hamilton, P. T. *Comb. Chem. High Throughput Screening* **2001**, *4*, 535−543.
(5) Rodi, D. J.; Makowski, L. *Curr. Opin. Biotechnol.* **1999**, *10*, 87−93.
(6) Gray, B. P.; Li, S.; Brown, K. C. *Bioconjugate Chem.* **2013**, *24*, 85−96.
(7) Li, S.; McGuire, M. J.; Lin, M.; Liu, Y. H.; Oyama, T.; Sun, X.; Brown, K. C. *Mol. Cancer Ther.* **2009**, *8*, 1239−1249.
(8) Hyde-DeRuyscher, R.; Paige, L. A.; Christensen, D. J.; Hyde-DeRuyscher, N.; Lim, A.; Fredericks, Z. L.; Kranz, J.; Gallant, P.; Zhang, J.; Rocklage, S. M.; Fowlkes, D. M.; Wendler, P. A.; Hamilton, P. T. *Chem. Biol.* **2000**, *7*, 17−25.
(9) Matsui, K.; Boniface, J. J.; Steffner, P.; Reay, P. A.; Davis, M. M. *Proc. Natl. Acad. Sci. U. S. A.* **1994**, *91*, 12862−12866.
(10) Hoofnagle, A. N.; Resing, K. A.; Ahn, N. G. *Annu. Rev. Biophys. Biomol. Struct.* **2003**, *32*, 1−25.
(11) Chalmers, M. J.; Busby, S. A.; Pascal, B. D.; West, G. M.; Griffin, P. R. *Expert Rev. Proteomics* **2011**, *8*, 43−59.
(12) Leurs, U.; Clausen, R. P.; Kristensen, J. L.; Lohse, B. *Bioorg. Med. Chem. Lett.* **2012**, *22*, 5811−5813.
(13) Szewczuk, L. M.; Culhane, J. C.; Yang, M.; Majumdar, A.; Yu, H.; Cole, P. A. *Biochemistry* **2007**, *46*, 6892−6902.
(14) Weis, D. D.; Engen, J. R.; Kass, I. J. *J. Am. Soc. Mass Spectrom.* **2006**, *17*, 1700−1703.
(15) Rand, K. D.; Pringle, S. D.; Morris, M.; Engen, J. R.; Brown, J. M. *J. Am. Soc. Mass Spectrom.* **2011**, *22*, 1784−1793.
(16) Rand, K. D.; Zehl, M.; Jensen, O. N.; Jorgensen, T. J. *Anal. Chem.* **2010**, *82*, 9755−9762.
(17) Leurs, U.; Lohse, B.; Rand, K. D.; Ming, S.; Riise, E. S.; Cole, P. A.; Kristensen, J. L.; Clausen, R. P. *ACS Chem. Biol.* **2014**, *9*, 2131−2138.
(18) Forneris, F.; Binda, C.; Vanoni, M. A.; Battaglioli, E.; Mattevi, A. *J. Biol. Chem.* **2005**, *280*, 41360−41365.
(19) Xia, G.; Boerma, L. J.; Cox, B. D.; Qiu, C.; Kang, S.; Smith, C. D.; Renfrow, M. B.; Muccio, D. D. *Biochemistry* **2011**, *50*, 93−105.
(20) Yan, X.; Broderick, D.; Leid, M. E.; Schimerlik, M. I.; Deinzer, M. L. *Biochemistry* **2004**, *43*, 909−917.
(21) Laskowski, R. A.; Luscombe, N. M.; Swindells, M. B.; Thornton, J. M. *Protein Sci.* **1996**, *5*, 2438−2452.
(22) Gron, H.; Hyde-DeRuyscher, R. *Curr. Opin. Drug Discovery Dev.* **2000**, *3*, 636−645.
(23) McDaniel, E. W.; Martin, D. W. *Rev. Sci. Instrum.* **1962**, *33*, 2.
(24) Iacob, R. E.; Murphy, J. P.; Engen, J. R. *Rapid Commun. Mass Spectrom.* **2008**, *18*, 2898−2904.
(25) Bennett, M. J.; Barakat, K.; Huzil, J. T.; Tuszynski, J.; Schriemer, D. C. *Chem. Biol.* **2010**, *17*, 725−734.
(26) Chen, Y.; Yang, Y.; Wang, F.; Wan, K.; Yamane, K.; Zhang, Y.; Lei, M. *Proc. Natl. Acad. Sci. U. S. A.* **2006**, *103*, 13956−13961.
(27) Klose, R. J.; Kallin, E. M.; Zhang, Y. *Nat. Rev. Genet.* **2006**, *7*, 715−727.
(28) Ng, S. S.; Kavanagh, K. L.; McDonough, M. A.; Butler, D.; Pilka, E. S.; Lienard, B. M.; Bray, J. E.; Savitsky, P.; Gileadi, O.; von Delft, F.; Rose, N. R.; Offer, J.; Scheinost, J. C.; Borowski, T.; Sundstrom, M.; Schofield, C. J.; Oppermann, U. *Nature* **2007**, *448*, 87−91.
(29) Hillringhaus, L.; Yue, W. W.; Rose, N. R.; Ng, S. S.; Gileadi, C.; Loenarz, C.; Bello, S. H.; Bray, J. E.; Schofield, C. J.; Oppermann, U. *J. Biol. Chem.* **2011**, *286*, 41616−41625.
(30) Lizcano, F.; Romero, C.; Vargas, D. *Genet Mol. Biol.* **2011**, *34*, 19−24.
(31) Weis, D. D.; Wales, T. E.; Engen, J. R.; Hotchko, M.; Ten Eyck, L. F. *J. Am. Soc. Mass Spectrom.* **2006**, *17*, 1498−1509.
(32) Fang, J.; Rand, K. D.; Beuning, P. J.; Engen, J. R. *Int. J. Mass Spectrom.* **2011**, *302*, 19−25.
(33) Percy, A. J.; Rey, M.; Burns, K. M.; Schriemer, D. C. *Anal. Chim. Acta* **2012**, *721*, 7−21.
(34) Jorgensen, T. J.; Gardsvoll, H.; Dano, K.; Roepstorff, P.; Ploug, M. *Biochemistry* **2004**, *43*, 15044−15057.
(35) Rand, K. D. *Int. J. Mass Spectrom.* **2013**, *338*, 2−10.
(36) Rand, K. D.; Zehl, M.; Jensen, O. N.; Jorgensen, T. J. *Anal. Chem.* **2009**, *81*, 5577−5584.
(37) Lohse, B.; Helgstrand, C.; Kristensen, J. B.; Leurs, U.; Cloos, P. A.; Kristensen, J. L.; Clausen, R. P. *PLoS One* **2013**, *8*, No. e67653.
(38) Terpe, K. *Appl. Microbiol. Biotechnol.* **2003**, *60*, 523−533.
(39) Smyth, D. R.; Mrozkiewicz, M. K.; McGrath, W. J.; Listwan, P.; Kobe, B. *Protein Sci.* **2003**, *12*, 1313−1322.